Heat transfer modelling of flashlamp heating for automated tape placement of thermoplastic composites

Anastasios Danezis [a,b,*], David Williams [b], Michael Edwards [b], Alexandros A Skordos [a]

[a] School of Aerospace, Transport and Manufacturing, Cranfield University, Cranfield, Bedford MK43 0AL, UK
[b] Heraeus Noblelight Ltd., Cambridge Science Park, Milton Road, Cambridge CB4 0GQ, UK

ARTICLE INFO

ABSTRACT

Flashlamp systems introduce pulsed and broadband heating to automated tape placement (ATP) offering greater control and optimisation potential. A thorough understanding of the role of operation parameters on the process is necessary to unlock these capabilities. A 2D finite element model of the heat conduction, able to analyse the temperature field evolution in the time scales of short high-energy pulses, was developed and combined with ray tracing analysis in this work. The model was validated against experimental data from ATP trials of AS4/PEEK composites. Parametric studies showed that pulse duration and frequency influence significantly both the surface and bulk temperature profiles. Longer pulses lead to higher irradiation temperatures, whilst the profiles converge to the behaviour of a continuous source of equivalent power at high frequency. The versatility of flashlamp heating enhances the processing envelope through expanding the feasible combinations of maximum temperature and depth of penetration achievable in ATP processing.

1. Introduction

Automated tape placement (ATP) is an additive manufacturing method which opens the way for the production of large composite parts in a single-step process. The method is very appealing for aerospace applications since the use of thermoplastic-based composites mitigates the need for long and costly autoclave cycles [1]. The in-situ consolidation capability of the process has not been fully utilised due to the challenges of meeting both quality and production criteria. Significant research effort has been carried out towards this direction in recent years [2].

The basic principle of ATP processing of thermoplastics is the deposition of layers of fibre-reinforced tapes by a moving placement head onto a tool. During the process, an energy source heats the new layer and the substrate before they come into contact at the nip point under a compaction roller. Maintaining the temperature within a pre-defined window is essential for the final quality of the part. Bond strength, crystallinity levels, void content and potential occurrence of thermal degradation depend strongly on the temperature history throughout the process [3–12]. The short timings involved in the placement process and the fact that the bonding zone is out of sight for part of the process make the monitoring and control of ATP challenging.

Thermal imaging can be utilised to measure surface temperatures outside the consolidation zone; however, a significant temperature drop occurs by the time the material arrives at the nip point due to shadowing [13–16]. In addition, the number of variables influencing the process is high and the heat transfer phenomena are inherently complex and non-linear, making it difficult to gain a thorough understanding based solely on experimental results.

Heat transfer analysis of the tape placement process has received considerable attention [17]. The majority of studies have focused on laser-assisted ATP of thermoplastic materials, specifically continuous carbon fibre reinforced polyether ether ketone (CF/PEEK). Models have also been developed to address the infrared (IR) heating of thermosetting composites [18–20]. Three-dimensional models have been used [21–23], but the problem is often reduced to two dimensions assuming uniform heating across the tape width and no edge effects [9,13,15,24–30]. Further simplifications can be made after examining the ratio of the advective to diffusive heat transport by means of the dimensionless Peclet number to establish if heat conduction in the placement direction can be considered negligible [13,16,31]. The contribution of exo/endo-thermic effects to the heat transfer during processing has been taken into account in some cases [9,24–26,28], while in others these effects have been considered negligible compared

---

to the heat source power input [13,15,16,23]. Most models use an Eulerian coordinate system following the placement head. Finite differences [16,24–26,31] and finite element [9,15,28,30] methods have been employed for solving the relevant boundary value problem.

The need for an accurate representation of thermal boundary conditions has motivated the development of optical models and the associated optical characterisation of composites. A number of studies have assumed constant heat flux acting on tapes, idealising the surface as a black body with total or partial light absorption [9,13,24,25,27]. Two-dimensional ray tracing models of the ATP cavity have been presented [13,15], whilst analyses based on the geometric view factor have been carried out for IR heating [18–20]. The angular and wavelength dependence of the reflectance of AS4/PEEK tapes has been measured [32] and used in 3D ray tracing models of laser-assisted ATP [15]. A better correlation of the predictions with the experimental data is achieved by taking into account the reflective and scattering behaviour of the composite [15].

Flashlamp systems are a recent addition to the available radiative sources for ATP applications. Unlike lasers and IR heaters, flashlamps emit broadband radiation and operate periodically, delivering high-energy pulses of several milliseconds which superimpose to heat the target surface. This mode of operation offers additional control capabilities compared to continuous heating. Besides the overall power output, the operating frequency and pulse duration determine the way the energy is delivered to the material. A wide parameter space is available offering greater process flexibility and opportunities for process tailoring. This advantage in combination with the fast response to operation changes, equivalent to lasers but superior to IR heaters known for residual heating, increases the potential for advanced process design and on-line control. Despite being as powerful as lasers, flashlamp systems require less stringent safety measures in the manufacturing area. Furthermore, flashlamps present an intermediate cost solution between IR lamps and laser-based systems, with the latter usually being associated with high acquisition and operation costs. To make use of these capabilities, a thorough understanding of the influence of operating parameters on the temperature field must be established. The short time scale of pulses imposes challenges to an experimental investigation of these effects, highlighting the need for models capable of describing the temperature field evolution. Efforts in this direction in an ATP environment have not been reported. Previous studies have benchmarked the capabilities to process thermoplastic and bindered dry fibre composites [33,34], whist a semi-empirical heat transfer model based on experimental estimates of the steady-state nip-point temperature for dry fibre materials has been used to analyse the process [35].

This paper presents a predictive modelling methodology of ATP using flashlamp heating, enabling the investigation of heat transfer mechanisms and of the influence of lamp parameters to be carried out. A 2D heat transfer finite element model of the process is developed and implemented with an appropriate formulation and assumptions for achieving computational efficiency. A three-dimensional optical ray tracing model of the lamp, reflective housing, light guide and the ATP cavity is used to provide accurate thermal boundary conditions. Experimental trial results are set against the outputs of the model and used to validate the latter over a range of conditions. The model is utilised to investigate the influence of the pulsed operation on the thermal field and to elucidate the way it can lead to improved processing of composites.

2. Methods

2.1. Heat transfer model

A finite element model of heat transfer during ATP processing under flashlamp heating has been developed in ANSYS 19.1 APDL. The prob-

lem was reduced to 2D assuming uniform heating across the tape width. An Eulerian frame was attached to the moving head with the material advection taking place through a fixed frame. The material movement is modelled by including advection to the energy balance:

$$\rho c_p \left(\frac{\partial T}{\partial t} + u_x \frac{\partial T}{\partial x} + u_y \frac{\partial T}{\partial y} \right) = \dot{q} + \frac{\partial}{\partial x}\left(k_x \frac{\partial T}{\partial x} \right) + \frac{\partial}{\partial y}\left(k_y \frac{\partial T}{\partial y} \right) \quad (1)$$

where ρ and c_p denote the density and specific heat capacity of the material, $\dot{q}$ the rate of heat generated or absorbed per unit volume, k_x and k_y the thermal conductivity and u_x and u_y the velocity components.

The $\dot{q}$ term accounts for the latent heat involved in crystallisation and melting of the thermoplastic matrix during processing. The crystallinity levels achieved in ATP are typically low due to the extreme cooling rates which can be over 2000 °C/min [9,24]. The heat released and absorbed as a result of these transformations is low for the nearly amorphous material. Moreover, the tapes are fibre-dominated with the polymer constituting only 30–35% of total tape mass. Therefore, the latent heat $\dot{q}$ is assumed to be negligible compared to the amount of energy provided by the heat source and the energy transfer introduced by the rapid material advection in the process.

The dimensionless Peclet number characterises the ratio of heat transfer by material motion to heat transfer by conduction:

$$Pe = \frac{uL}{a} \quad (2)$$

where L is a characteristic length, u the velocity of the material flow and a the thermal diffusivity. Deposition rates in ATP usually exceed 50 mm/s, whilst the axial thermal diffusivity of typical thermoplastic-based composites is in the $1–10 \times 10^{-6}$ m^2/s range, typically around 2×10^{-6} m^2/s for AS4/PEEK. For a processing length as short as the roller diameter, the Peclet number is of the order of 10^3. The high values of the Peclet number mean that the thermal field in the placement direction is strongly governed by material advection, whilst the contribution of heat conduction within the tape is very small. Low velocities during the first moments of the process can result in Peclet numbers lower than unity. However, this condition is true for a very short period compared to the duration of the placement process. Eq. (1) can be simplified further also taking into account that material motion is aligned to the local x-coordinate:

$$\rho c_p \left(\frac{\partial T}{\partial t} + u_x \frac{\partial T}{\partial x} \right) = \frac{\partial}{\partial y}\left(k_y \frac{\partial T}{\partial y} \right) \quad (3)$$

In a problem expressed by Eq. (1), the finite element solver imposes limitations on the mesh size to diminish the possibility of solution oscillations and lack of convergence [36]. This amounts to ensuring the Peclet number is lower than 1, where in this case the characteristic length (L) is equal to the element size in the direction of movement. If the solution is carried out following Eq. (1), with values of thermal diffusivity corresponding to those in the fibre direction of the tape, the mesh size in the direction of the movement should be kept lower than 10 μm at 100 mm/s. This results in a very high number of nodes rendering the model highly inefficient. Given that the physics of the problem is represented accurately by the simplified form of the energy balance expressed by Eq. (3), the value of the thermal conductivity in the direction of the movement of the tape does not play a role as long as it is below a limit which maintains a relatively high value of the Peclet number of the macroscopic movement for characteristic lengths corresponding to the diameter of the roller. Increasing the thermal conductivity in the direction of the fibre by a factor of 10 still maintains high values of the Peclet number, in the order of 10^2, while allowing the Peclet number corresponding to the mesh size to have a low value for element dimensions around 100 μm, thus preserving a good level of stability of the solution. Therefore, the conductivity in the fibre direction

(k_x) is increased artificially by a factor of 10 in the model implementation to achieve an accurate and stable solution, while keeping solution times within acceptable limits. The impact of the increased in-plane conductivity on model results was examined, and no influence was found.

The model represents the composite tapes, the deformed elastomeric roller and the aluminium tool (Fig. 1a). The feed angle of the incoming tow (e), the roller diameter (D) and the length of deformation (B) correspond to the configuration used in experimental trials. The substrate comprises three AS4/PEEK 0.18 mm layers, whilst the thickness of the roller and the tool have been reduced to 2 mm to decrease the number of elements in the analysis, without affecting the solution.

The high heat flux applied during a pulse imposes a through-thickness element size of 10 μm for the composite tapes. Refining a thin material slice close to the surface is sufficient to reach convergence if the thickness for the fine mesh region exceeds the thermal penetration depth of the pulse. The temperature varies periodically within the region defined by the penetration depth and represented by a fine mesh. Outside this area, the periodic temperature variations become negligible and the temperature reaches a steady state that can be captured accurately by a coarser mesh with element thickness of 10–200 μm. The size of the refined zone should exceed the penetration depth of a periodic source, which is [37,38]:

$$d_p = \sqrt{\frac{2a}{\omega}} \qquad (4)$$

where ω is the angular frequency of the pulse.

For the frequencies used in this work (25–100 Hz) and transverse thermal conductivities of the tapes, which are in the 0.4–0.8 W/m/°C range, the values of penetration depth are in the 30–80 μm range. A thickness of 180 μm for the fine mesh zone was used across the substrate and tow in all simulations, which exceeds the maximum of the penetration depth range by a factor of two. The rest of the substrate, roller and tool were represented by a coarser mesh. The resulting mesh is illustrated in Fig. 2.

The thermal boundary conditions applied are illustrated in Fig. 1a. The material moves through the analysis frame with a velocity equal to the ATP processing speed. Across the curved parts, the velocity is assigned to each element based on the radial distance and angular velocity. An ambient temperature of 25°C is assigned to the nodes occupying the entry edges of the composite and aluminium tool (S_{IN}). This temperature value can be adjusted accordingly if a heated tool is deployed. For the elastomeric roller entry nodes, the value is set at 50°C to account for the residual roller heating during continuous processing. The impact of this condition on the predicted nip-point temperature has
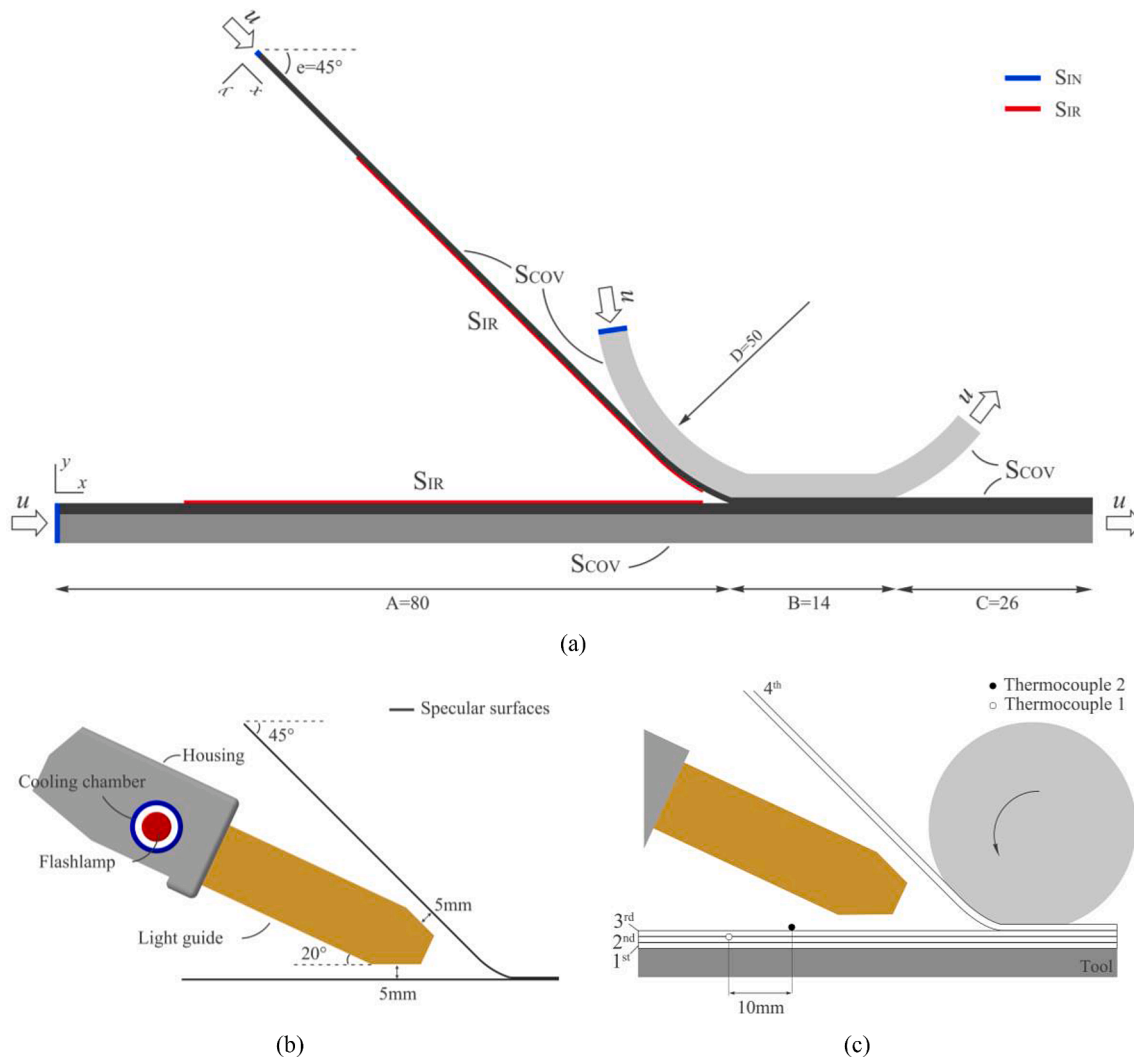

Fig. 1. Process representation: (a) heat transfer model geometry, dimensions and regions of boundary conditions. Lengths are in mm; (b) schematic of the flashlamp ATP configuration modelled using ray tracing; (c) schematic of the ATP process used in the manufacture trials of AS4/PEEK composites. (For interpretation of the references to colour in this figure legend, the reader is referred to the web version of this article.)
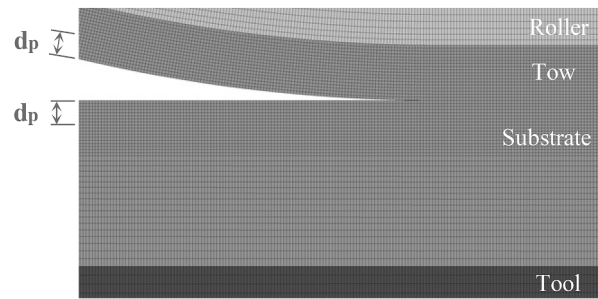
Fig. 2. Detail of the substrate, tow and roller mesh at the nip point. The composite parts feature zones of finer mesh near the surface which exceed the expected thermal penetration depth (d_p). (For interpretation of the references to colour in this figure legend, the reader is referred to the web version of this article.)

been shown to be weak [14].

The boundaries denoted as S_{COV} are subjected to forced convection due to laminar air flow. The average convection coefficient across the boundaries is [39]:

$$h = \frac{k_{air}}{L} 0.664 \ Re_x^{1/2} Pr^{1/3} \tag{5}$$

where Re_x is the Reynolds number of the air flow corresponding to the velocity of the tapes and Pr and k_{air} are the Prandtl number and thermal conductivity of air respectively. A length scale (L) of 0.05 m is used for the model. The properties of air are calculated for the average value of the ambient T_{amb} and element surface temperature T_{sur} in every time step during the solution.

A combined irradiation ($q_{(x,t)}$) and convection boundary condition is applied to the S_{IR} boundaries:

$$k_y \frac{\partial T}{\partial y} = q_{(x,t)} - h(T_{sur} - T_{amb}) \tag{6}$$

The convection coefficient for the substrate follows Eq. (5). Forced and natural convection act simultaneously on the incoming tow due to the inclined position. The coefficient is calculated for the feed angle of the tow using a relation derived for an inclined semi-infinite isothermal plate [40].

The pulsed operation is modelled by periodically activating the heat flux term $q_{(x,t)}$ in Eq. (6) as dictated by the operating frequency (f) and pulse duration (d) of the system. The heat flux value applied to each element over the S_{IR} boundaries is determined by the system power output and the ray tracing model presented in the following section. The spatial irradiance distribution across the tape width is reduced to a single profile due to the 2D domain of the model, which is an average of five profiles around the tape central line. The profile is interpolated to account for the different meshes between the optical and thermal models. Assuming a rectangular waveform, the average power $\overline{P}$ the flashlamp delivers is:

$$\overline{P} = P_f f d \tag{7}$$

where P_f is a characteristic power value derived using the voltage and current of the lamp during a pulse.

The fraction of electrical power converted to optical output power for a flashlamp is determined by numerous parameters such as the lamp design, gas pressure, the driving conditions and power supply architecture. To render the methodology developed applicable to a wide range of flashlamp systems and operation parameters, a factor of 0.5 was assumed which is typically used for Xenon flashlamps [41,42].

The material properties used for the analysis are presented in Table 1. The conductivity and volumetric heat capacity of the AS4/PEEK

Table 1
Thermal properties of the AS4/PEEK prepreg, roller and tool used in the analysis [43,44].

Material/ Temperature	Specific heat capacity (J/kg/K)	Transverse thermal conductivity (W/m/K)	Density (kg/m^3)
AS4/PEEK [43]	[43]	[43]	[44]
0°C	749	0.38	1601
50°C	983	0.44	1598
100°C	1198	0.51	1593
150°C	1386	0.57	1593
200°C	1559	0.64	1586
250°C	1715	0.70	1575
300°C	1852	0.76	1563
350°C	1985	0.68	1537
400°C	2081	0.65	1524
Elastomer	1255	0.25	1250
Aluminium	950	237.5	2700

over a range of temperatures are reported in [43] based on inverse solutions. The values are in good agreement with previous measurements performed by two laboratories [13]. The specific heat capacity required as an input for the finite element analysis is derived from the volumetric data [43] and the temperature-dependent density of AS4/PEEK tape [44].

The simulation time is discretised into load steps with sufficiently short duration to model individual pulses. A minimum of two load steps per period are required to describe the pulsed operation; one covering the pulse event and one the remaining period. The time increments within each load step are adjusted by the software to achieve convergence. This is carried out using a Newton-Raphson scheme with iterations continuing until the square root of the sum of the squares (SRSS) of the residual vector is lower than the SRSS of 0.1% of the applied loads or 10^{-9}, whichever is greater.

The mesh comprises approximately 400,000 quadrilateral 4-node elements (PLANE55). The analysis goes through a transient phase before all node temperatures reach a periodic steady state. This is accomplished after 2 s for the examined geometry at a processing speed of 50 mm/s and 50 Hz operating frequency, which translates to about 1 h of computational time on a 4-core desktop PC. The running time increases with frequency since the number of load steps for covering the solution time is greater.

2.2. Optical model

A three-dimensional ray tracing model of the flashlamp system in an ATP process has been developed in TracePro LC 7.5.3 [45]. The model includes the cavity formed by the composite tapes and a number of

system components: the flashlamp tube, a water-filled cooling chamber, the quartz light guide and the reflective housing which holds the assembly in place (Fig. 1b). The system head is mounted close to the cavity with the light guide edges being 5 mm away from each tape. Similar methodologies for lasers have modelled the source as a collimated or divergent beam which originates from a virtual point and irradiates the cavity. The different working principle of the flashlamp system and position inside the process render equivalent assumptions not applicable. The light output is not known beforehand but shaped by the interaction of light with system components and the distance from the target surfaces.

The composite tapes are represented as highly absorbing surfaces with specular reflections. The tapes have the same geometry as in the 2D thermal model with a width of 25 mm. The transmittance of CF/PEEK tapes has been found to be below 0.1% over the 500–2000 nm range [32], whilst PEEK is highly absorptive over the 200–500 nm wavelength range. Therefore, it is valid to consider the transmittance of the material negligible across the flashlamp spectrum, which lies on the 200–1000 nm range according to spectral measurements. Light reflections are assumed specular and described by the Fresnel equations with an angular dependence which corresponds to a refractive index of 1.95, which yields a good agreement with experimental results [32]. Measurements at different wavelengths have shown only a 2% increase of reflectivity between 500 nm and 1000 nm [32]. To simplify the analysis, a source surface model with angular dependence over the whole flashlamp spectrum was used. The models and properties used for the rest of the parts in the model are summarised in Table 2.

The ray tracing technique solves the optical problem by generating a large number of rays and calculating their paths through the different optical media. A Lambertian source flux model with characteristic flashlamp emission spectra was used to describe the flashlamp, which distributes the power uniformly over the tube surface area. The rays are emitted from the surface at random positions whilst having a cosine-weighted angular distribution. Each ray carries a small portion of the total energy provided by the source. The composite surfaces (substrate and the incoming tow) are divided into grids of 60×60 data cells which capture the energy delivered by the incident rays to calculate irradiance values. Ten million rays were required to achieve statistical convergence of the solution. The model provides the irradiance distribution on the tow and substrate as a result of a single irradiation event. The pulsed operation of the lamp is represented by scaling the solution over time at appropriate times to produce pulses of specific duration and frequency.

2.3. Validation trials

Manufacturing trials of AS4/PEEK composites were performed at the University of Leoben, Austria to validate the model predictions. The available robot cell featured an ATP head, comprising a tape feeding unit and a roller, capable of placing 1-inch thermoplastic tapes on a metallic moving tool which measures 700 mm × 350 mm [48]. A Heraeus Noblelight *humm3*™ flashlamp system [49] of 4.4 kW maximum

Table 2
Constitutive models and properties used in the optical modelling of the flashlamp source.

Material	Model/Assumptions	Input properties	Source
AS4/PEEK	Partially absorbing surface with specular reflections	Absorptance Reflectance	[32]
Water	Complex refractive index Absorption coefficients by Lambert's law	Refractive index Extinction coefficients	[46]
Aluminium	Partially absorbing surface with specular reflections	Absorptance Reflectance	[47]
Quartz (Fused silica)	Extended Schott equation	Refractive index	TracePro Database [45]

average electrical power was deployed as the heating source. The selected light guide design and positioning relative to the material surfaces for these tests are illustrated in Fig. 1b.

Four-ply 25 mm wide AS4/PEEK specimens were fabricated by operating the flashlamp at three different frequencies: 25, 50 and 100 Hz with the pulse duration being compensated to 4.75 ms, 2.25 ms and 1.1 ms respectively to achieve maximum power output (Eq. (7)). The processing speed was 50 mm/s. The first ply was held on the tool using high temperature tape at the ply ends. Thermal profiles on the substrate surface and one ply below were acquired by 75 μm diameter K-type thermocouples during the deposition of the 4th ply (Fig. 1c). The thermocouples were placed in the centre of the substrate and 10 mm apart to minimise their effect on the thermal field and local thickness. An Omega Engineering OM-DAQ-USB-2401 acquisition module was used with a sampling frequency of 150 Hz to capture the temperature data.

3. Results and discussion

3.1. Optical model irradiance predictions

The predicted irradiance in the ATP cavity as a result of a single irradiation is illustrated in Fig. 3. The values correspond to a total of 2.2 kW optical power which is delivered by the incident rays. The area of maximum irradiance is located approximately 20–30 mm away from the nip point for both the substrate and tow, due to the position of the chamfered edges of the light guide. A high number of rays escape at these edges which reinforces the importance of including the light guide geometry in the optical model. Few rays reach deeper into the cavity due to its shape, with the irradiance values dropping to zero values at the nip point.

The spatial distributions were reduced across the tape width to a single irradiance profile which is the average of five profiles around the tape central line. The Savitzky-Golay filter was employed to smooth the data and eliminate outliers caused by the statistical nature of the solution (Fig. 4). The coefficients of determination R^2 achieved were over 0.98 for both the substrate and tow.

3.2. Thermal model predictions and validation

The distributions of temperature predicted by the model for the 25 Hz 4.75 ms case, 0.52 s and 2 s after the start of the analysis, are illustrated in Fig. 5. As the process progresses, material moves throughout the analysis frame diffusing heat from the irradiated region to the consolidation and ambient parts of the process. Simultaneously, heat diffusion to deeper material levels takes place. The temperature field enters a periodic steady state after 2 s with a period corresponding to the frequency of the flashlamp operation. Because of the fixed analysis frame, the model prediction provides the temperature field in a span of 0.12 m (total model length) in the movement direction, at a given time from the start of the layer deposition. Superimposing the thermal fields predicted for the consecutive time steps composes the overall temperature history along the corresponding processed length of material.

The profiles obtained during manufacturing trials and the corresponding model predictions are presented in Fig. 6. The model profiles correspond to the temperature history of a single point which moves at 50 mm/s on the substrate surface, or at one layer depth, throughout the analysis frame. A surface point enters the irradiation region of the process 1.2 s before approaching the nip point which is reached at a time of 0 s (Fig. 6a, c, e). The point is exposed to multiple irradiations as the time to cross the irradiation zone (1.2 s) is greater than the pulse period (10–40 ms). As a result, the point is subjected to a series of heating/ cooling cycles with the repetition time (t_p) equal to the flashlamp operation period as observed in Fig. 7. The heating phase duration of each cycle (t_h) is equal to the duration of incoming energy pulses by the flashlamp, whilst cooling at ambient conditions occupies the remaining
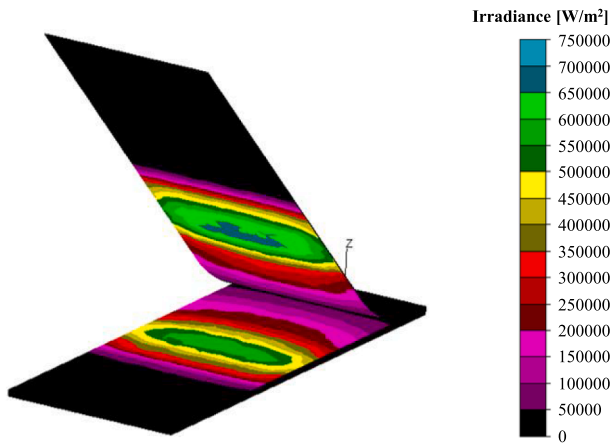
Fig. 3. Irradiance predicted by the optical model in the ATP cavity as a result of single irradiation event. The values given correspond to system optical power of 2.2 kW. (For interpretation of the references to colour in this figure legend, the reader is referred to the web version of this article.)

not irradiated directly in the consolidation and ambient parts of the process and the predictions present a maximum deviation of 10% in all cases. The temperature profiles predicted by the model at one layer depth are higher, up to 50°C, than those captured by Thermocouple 1. It is attributed to the poor consolidation, as a result of the processing temperatures being significantly lower than the melting point of PEEK at 340°C, which caused imperfect contact of the thermocouple with plies 2 and 3 (Fig. 1c). The predictions show good agreement once it enters the consolidation zone where the roller applies additional pressure to the plies.

3.3. Process sensitivity to frequency and pulse duration

The predicted temperature profiles of a surface point for the 25, 50 and 100 Hz cases are illustrated in Fig. 8. The prediction for a continuous source of equivalent electrical power (4.4 kW), efficiency and irradiance on the tapes is added for comparison. The flashlamp achieves significantly higher temperatures in the irradiation stage for the same average power. This is because the system delivers an order of magnitude higher power during each pulse event, which is compensated by the remaining period of time to eventually result in equivalent average power to the continuous source. The duration of the pulse plays a major role in the maximum values of temperature reached. In particular, a 4.75 ms pulse results in up to 50, 100 and 150°C higher peak temperatures compared to the 2.25 ms, 1.1 ms and the continuous cases respectively. At the end of each operation period, all pulsing scenarios drop below the continuous operation. The cooling of the surface appears greater at lower frequency due to the longer time intervals between consecutive irradiations. In addition, the flashlamp frequency determines the number of heating/cooling cycles a surface point is exposed to across the irradiation part of the process. The short operating period of the 100 Hz scenario leads to four times greater number of cycles in comparison to the 25 Hz case. In the irradiation region, the flashlamp profile converges to the continuous one with increasing frequency. For the rest of the processing cycle, the profiles are nearly identical despite the significantly different operating conditions. In this region, the differences are lower than 10°C as a result of the use of equivalent average power. The effect of the pulse duration decoupled from frequency is presented in Fig. 9 in which the frequency is constant at 25 Hz. In this case, changes in pulse duration affect the average power linearly following Eq. (7) with a sensitivity of 0.9 kW/ms. The surface temperature profiles are shifted to
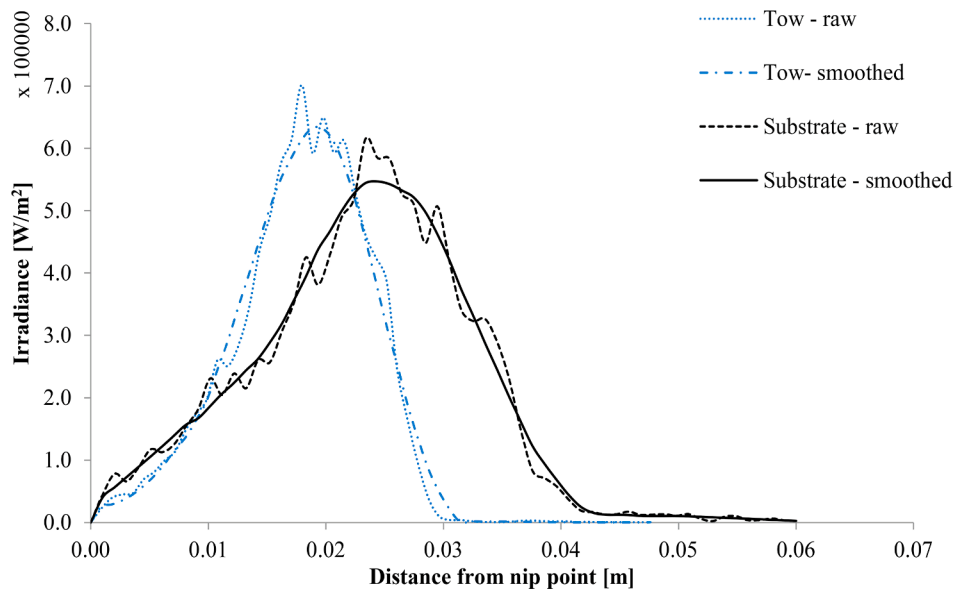
period. These effects are reproduced in detail by the model as a result of the fine time discretisation. Although Thermocouple 2 is located on the substrate surface, it cannot capture these effects due to their short timescale compared to the sensor response time, approximately 0.05 s according to the manufacturer [50]. The recorded values are effectively an average of the surrounding temperature field on the composite surface. At the nip point region, a steep temperature increase occurs when the substrate and heated tow come into contact and exchange heat rapidly. The interface is then consolidated underneath the roller for 0.28 s and subjected to ambient conditions for the rest of the processing cycle. The irradiation is registered with a noticeable delay one layer below the surface (Fig. 6b, d, f) due to the low transverse thermal conductivity of the composite. At this depth, the heat transfer between the composite parts is seen as a secondary temperature peak at a time of about 0.05 s successfully reproduced by the model.

The model predictions correlate well with the experimental data in terms of events timing and values. In the irradiation stage, the profile of Thermocouple 2 is close to the mid-level of the temperature range the surface point experiences according to the model. The thermocouple is

Fig. 4. Irradiance profiles on the substrate and tow after the reduction of the spatial distribution across the tape width to a single profile. The Savitzky-Golay filter was applied for smoothing the data. (For interpretation of the references to colour in this figure legend, the reader is referred to the web version of this article.)
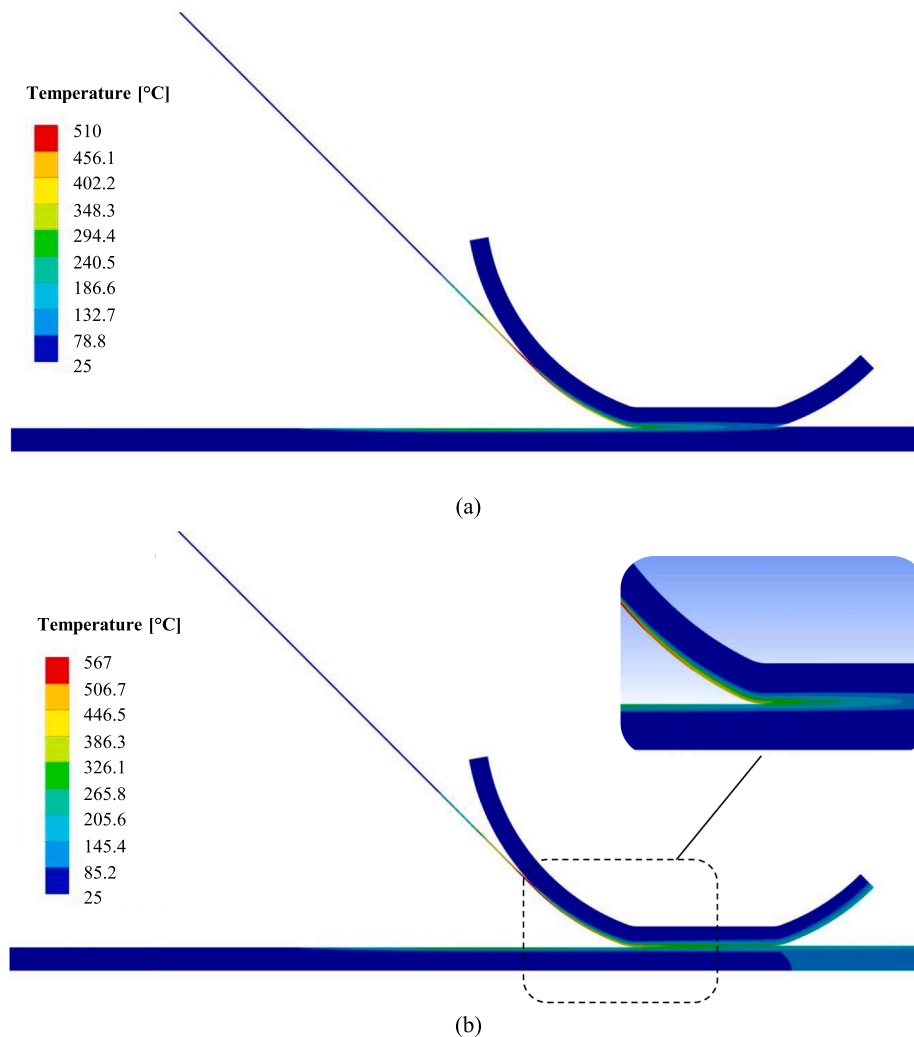
(a)

(b)

Fig. 5. Colour maps of the predicted temperature field across the model for the 25 Hz 4.75 ms case: (a) 0.52 s and (b) 2 s after the start of the analysis. (For interpretation of the references to colour in this figure legend, the reader is referred to the web version of this article.)

higher levels with increasing pulse duration, with a sensitivity of about 50°C/ms.

The temperature distribution in the substrate under irradiation for the 25 Hz, 100 Hz and continuous cases is given in Fig. 10, 25 mm before the nip point. Profiles at the end of the pulse event and the period are given. An intermediate state is also reported for the 25 Hz case, 8.9 ms after the end of the pulse, to compare with the temperature distribution of the 100 Hz scenario at equal timings. The pulses result in an increase of the surface temperature with the profile decreasing significantly with depth compared to the continuous operation. At the end of the heating phase, the 25 Hz case reaches higher temperatures than the 100 Hz one at a depth of approximately 100 μm. After 8.9 ms, significant heat diffusion towards the material bulk has occurred, especially for the 25 Hz scenario. At this point, the cycle of the 100 Hz case has been completed and the next energy pulse is delivered on the surface. On the other hand, the diffusion of the 25 Hz case continues for 26.35 ms and as a result the surface cools down more. Deeper material levels are affected in this stage. The two extreme temperature distributions of each heating/cooling cycle intersect at a position which represents the thermal penetration depth approximated using Eq. (4). In contrast, the profile of

the continuous source does not present similar variations with time and the bulk temperatures can be influenced only by the heat flux applied on the surface for given material properties. The profiles of the pulsed and continuous cases almost coincide beyond a depth of 100 μm. Therefore, the flashlamp offers additional control over the maximum temperatures in the 0–100 μm depth range for the specific material and pulsed conditions tested. Operation scenarios of lower frequency and longer pulses result in higher surface and bulk temperatures but these do not exist simultaneously, presenting time differences which are determined by the depth and the material conductivity in this direction. As frequency increases, lower depths are affected and the temperature range between the extreme states becomes narrower converging to the continuous operation.

The results presented show that the flashlamp offers additional control capabilities. In the case of continuous sources such as lasers, the temperature profiles in the irradiation stage can be controlled by physically altering the incident angle of the beam or the source power. However, both strategies are expected to have secondary effects in other parts of the process. Changes in the source power affect the temperatures on the substrate during the irradiation as well as the bond line
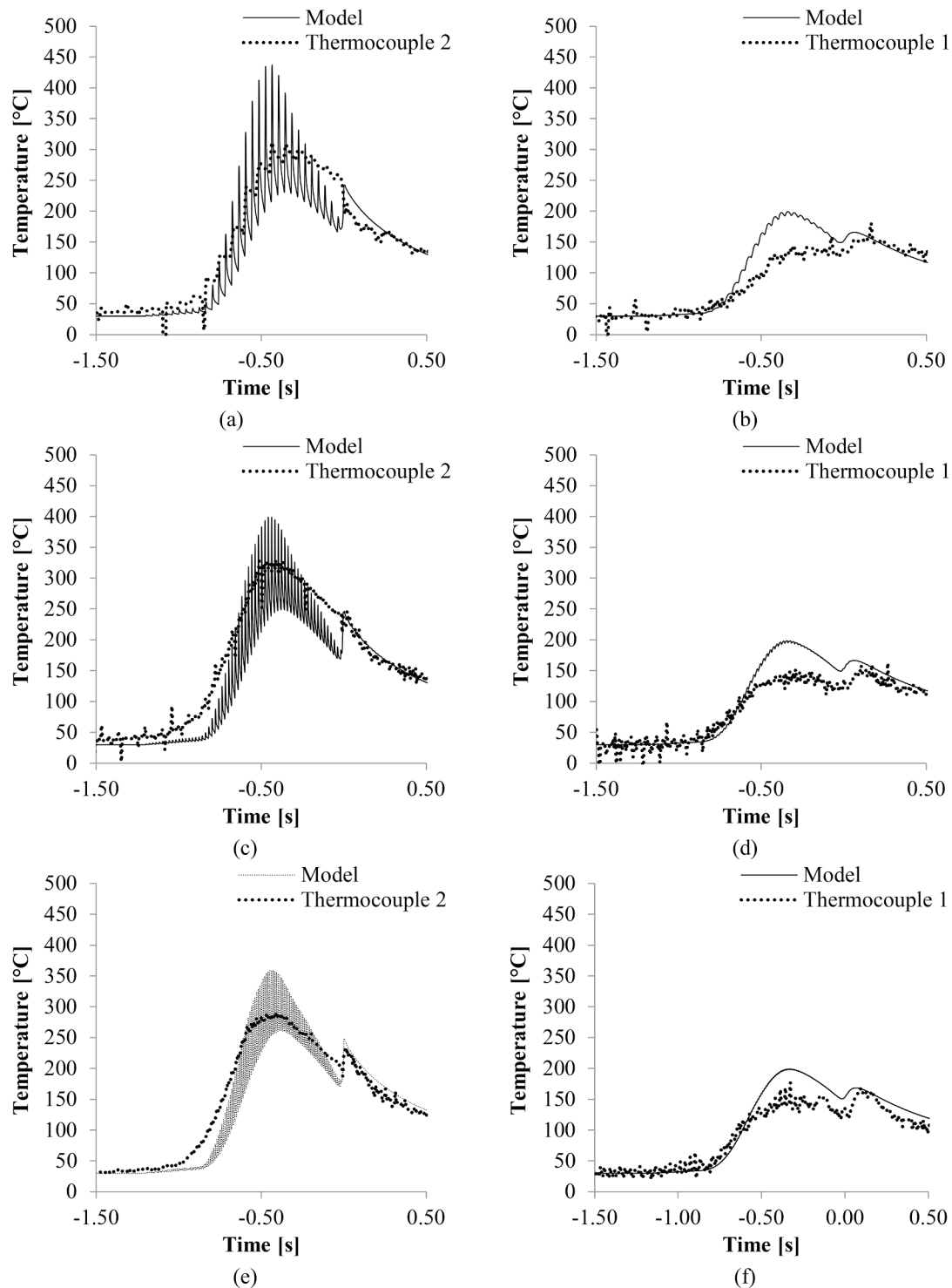
Fig. 6. Validation of heat transfer model of the ATP process against experimental temperature measurements: (a) 25 Hz 4.75 ms substrate surface; (b) 25 Hz 4.75 ms one layer depth; (c) 50 Hz 2.25 ms substrate surface; (d) 50 Hz 2.25 ms one layer depth; (e) 100 Hz 1.1 ms substrate surface; (f) 100 Hz 1.1 ms one layer depth. (For interpretation of the references to colour in this figure legend, the reader is referred to the web version of this article.)

temperatures. In contrast, the pulsed operation unlocks additional optimisation routes. The maximum surface temperatures during the irradiation stage (Fig. 8), as well as the affected material depth and bulk temperatures (Fig. 10), can be adjusted by setting the pulsing conditions appropriately whilst maintaining equivalent bond line temperatures. This is an important feature since the temperature history prior to the nip point determines the crystallinity levels and degree of melting

achieved, whilst it can also lead to thermal degradation if the values of temperature exceed a threshold. In addition, the fact that the field converges to that of a continuous source at high operating frequencies indicates the versatility of the flashlamp to achieve different process outcomes as the source can produce conditions close to a continuous source but also reach outcomes which are not feasible under continuous heating.
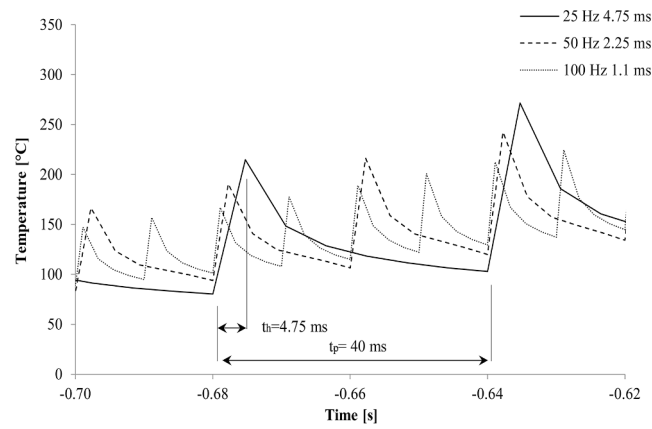
Fig. 7. The heating/cooling cycles developed on the substrate surface for the different pulsing scenarios. The relevant timings are explicitly noted for the 25 Hz frequency 4.75 ms duration pulse. (For interpretation of the references to colour in this figure legend, the reader is referred to the web version of this article.)
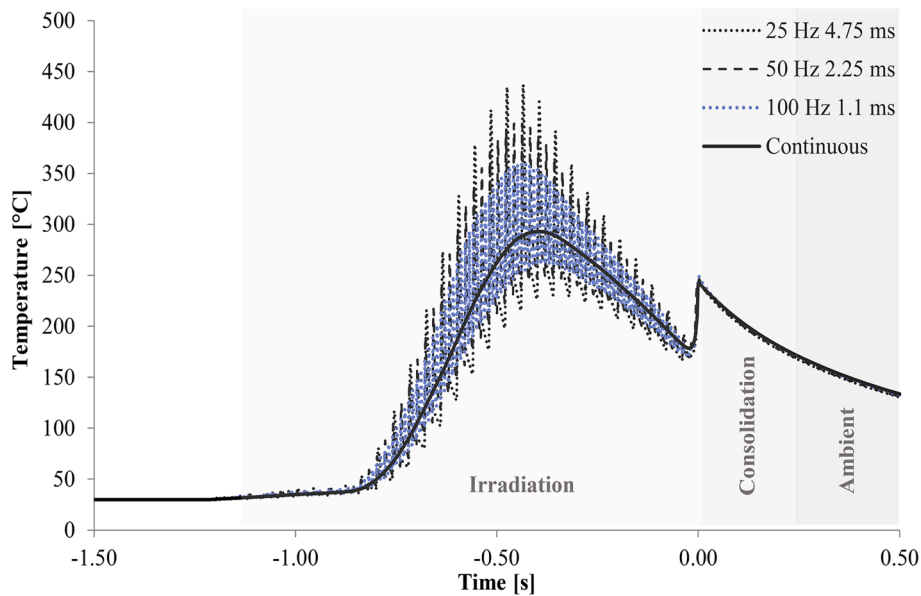

Fig. 8. Comparison of the predicted surface temperature profiles across the process stages for the 25 Hz, 50 Hz and 100 Hz scenarios. The profile of continuous equivalent power (4.4 kW) is also shown. (For interpretation of the references to colour in this figure legend, the reader is referred to the web version of this article.)

3.4. Process sensitivity to deposition rate

Fig. 11 illustrates the dependence of the nip point temperature on the process rate. As velocity increases, the temperature for the three pulse cases and continuous irradiation diminish in a non-linear way. The values coincide for all operations as a result of featuring equivalent average power. The corresponding maximum temperatures achieved at the end of the pulse on the substrate and tow are given in Fig. 12. The flashlamp heating achieves significantly higher temperatures during the irradiation stage. Longer duration pulses, and subsequently lower frequencies, lead to greater maximum temperatures for the whole range of velocities. The temperatures on the tow surface are higher than the substrate due to the higher irradiance values predicted by the optical model (Fig. 4) and its lower thickness. The sensitivity of the maximum

temperatures to the processing rate is different for the substrate and tow with the latter experiencing higher temperatures drops for equal velocity increments. In particular, the temperature drop at 25–50 mm/s is approximately 300°C on the tow for all operations while it is only 60°C for the substrate. At 25 mm/s, the tow temperatures under all operations exceed the thermal degradation threshold of the material at 600°C. The effect of degradation is in general time-dependent [9,12] making it possible for the material to withstand higher temperatures for shorter exposures. Currently, there is no available information in the literature on the degradation kinetics of the material used here in such short time scales.
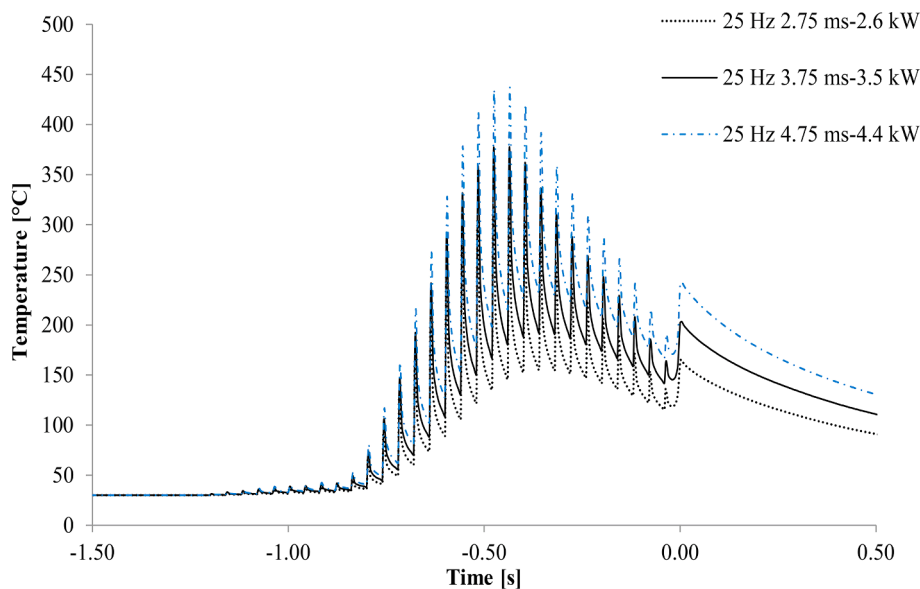
Fig. 9. Effect of the pulse duration under constant frequency of 25 Hz on the surface point temperature profile and average power value. (For interpretation of the references to colour in this figure legend, the reader is referred to the web version of this article.)
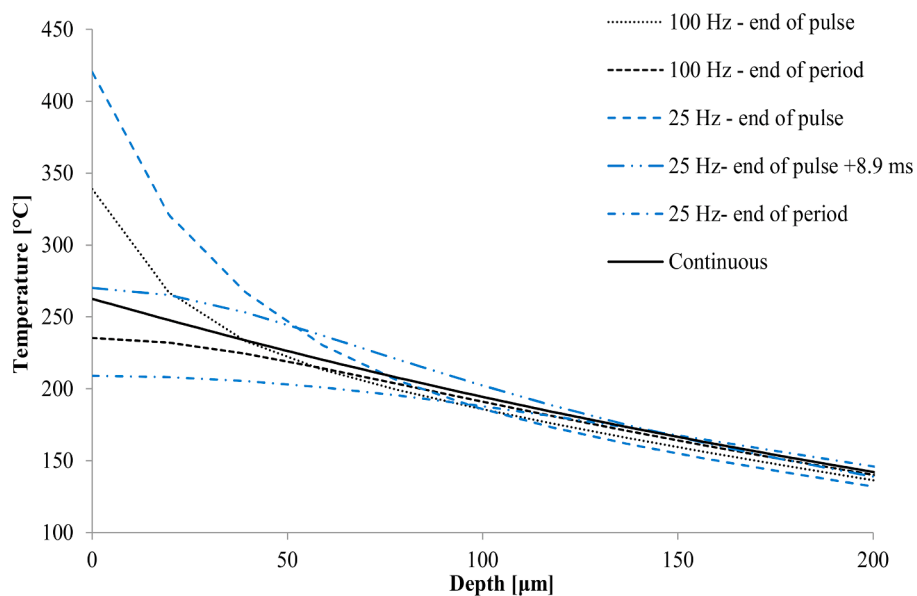

Fig. 10. Evolution of through-thickness temperature profiles in the substrate during a single operating period for the 25 and 100 Hz pulse cases, 25 mm before the nip point. (For interpretation of the references to colour in this figure legend, the reader is referred to the web version of this article.)

3.5. Process envelope

Under flashlamp heating, material points do not necessarily follow identical heating and temperature histories throughout the processing cycle. The magnitude of this effect depends on the combination of frequency and processing rate, which can cause consecutive pulses to be applied with a distance on the tape, with the effect intensifying at lower frequencies and greater velocities. Insufficient overlap of the energy pulses, in conjunction with the variable irradiance across the heated zone, creates variations in irradiation conditions. The bond line is indirectly affected since material regions with different temperature histories arrive at the nip point; however, this effect diminishes deeper into the consolidation region. The effect is negligible for the low processing rates presented in previous sections, but it is more pronounced in Fig. 13 for the 25 Hz 4.75 ms operation at 500 mm/s, where the

temperature history of five points located 5 mm apart on the substrate surface is given. In this case, the irradiation zone starts at a time of 0.12 s and the surface points are exposed to fewer irradiations than at 50 mm/s (Fig. 8). The five points go through different temperature maxima, with differences up to 100°C, as well as different irradiation timings relative to the nip point. Furthermore, the bond line temperatures are not identical for all points but oscillate within a range of up to 15°C. Points 1 and 5 in Fig. 3 are 20 mm apart, which corresponds to the distance covered between consecutive pulses, the product of 0.4 s operating period and 500 mm/s processing rate. These points go through similar heating conditions and thus their temperature profiles coincide. The temperature profiles presented in Fig. 13 repeat periodically on the substrate surface every 0.4 s or 20 mm in this case.

The differences in temperatures and irradiation times before the nip point can affect the melting/crystallisation of the composite matrix.
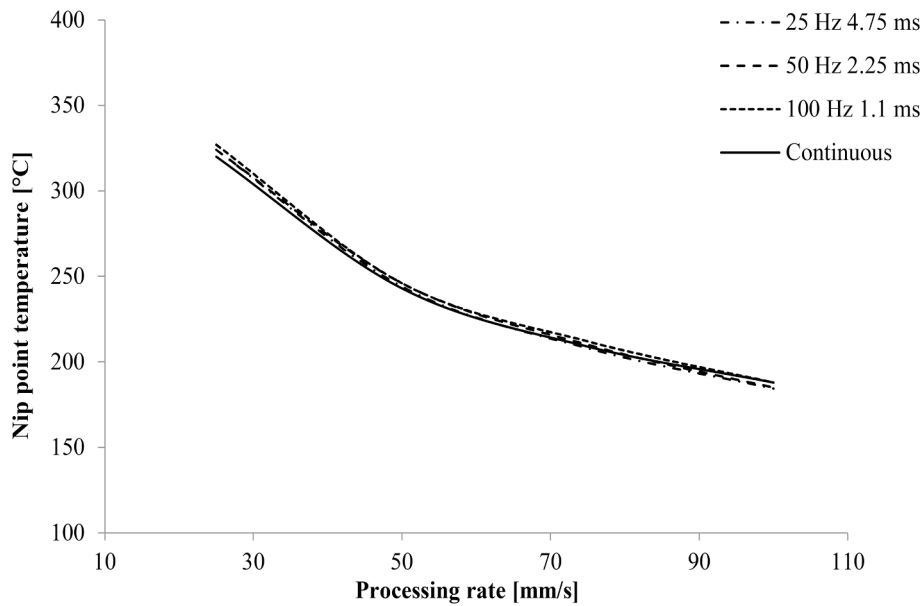
Fig. 11. Nip-point temperature dependence on process rate for the 25 Hz 4.75 ms, 50 Hz 2.25 ms, 100 Hz 1.1 ms and contiunuous operations.
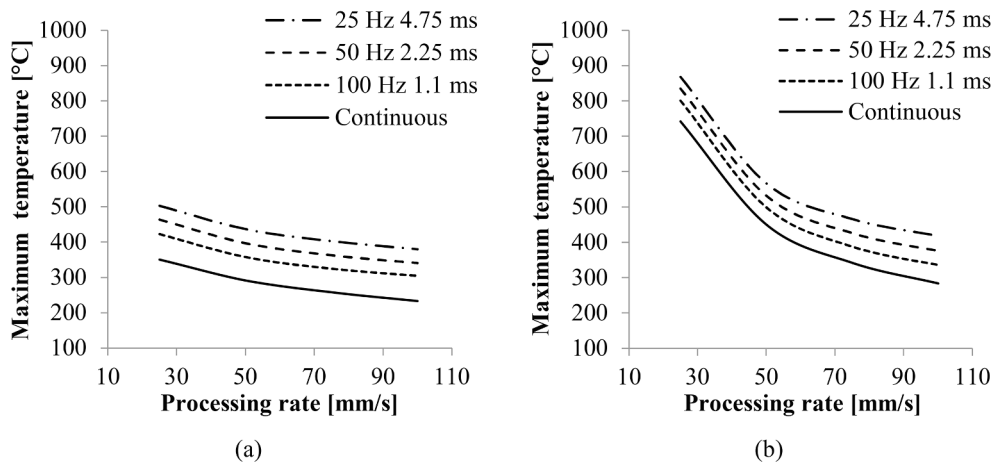

(a)

(b)

Fig. 12. Dependence of (a) substrate and; (b) tow maximum surface temperature on processing rate.

Similarly, the oscillations of the bond line temperatures could lead to non-uniform bonding development across the processed length. The process design space can be narrowed to eliminate these effects by defining the critical velocities as a function of frequency over which significant temperature variations occur. The velocity at which differences greater than 5, 10 and 20°C appear among the surface points during the irradiation or across the bond line were determined for the 25, 50 and 100 Hz cases for the configuration of this study at 4.4 kW average power. The temperature history of 1000 points on the substrate surface was examined in a span equal to the distance covered between consecutive pulses. The map of limit frequency and velocity conditions for 5, 10 and 20°C variations is illustrated in Fig. 14. For each case, the points form a line in the frequency-speed space, which defines the feasible processing envelope in which the process conditions result in practically uniform heating across the material according to the acceptable temperature variations. Combinations of operating frequency and velocity outside the shaded area result in greater variations. Use of such a map is necessary to select appropriate flashlamp settings and process conditions and simulation presents an efficient way to obtain the underlying information.

4. Conclusions

A predictive modelling methodology of ATP under flashlamp heating was presented in this study, enabling the investigation of the operation parameters role on the transient temperature field. A 2D heat transfer finite element model of the ATP process was developed and combined with ray tracing methods which provided boundary conditions of irradiance on the materials. Good agreement was found between the predicted temperature profiles and experimental data. The effect of the operation parameters was found to be significant on both the surface and bulk temperatures, especially during the irradiation phase of the process. The model predictions revealed trends not possible to capture experimentally, due to the short timings involved, highlighting the need for process design based on heat transfer modelling.

The results of this study show that flashlamp heating offers the potential of improved outcomes since the adjustable operation adds another layer of temperature control in the process. The simulation provides an efficient method to investigate the thermal field and optimise it. Some combinations of velocity and frequency result in non-uniform heating; however, these effects can be eliminated by
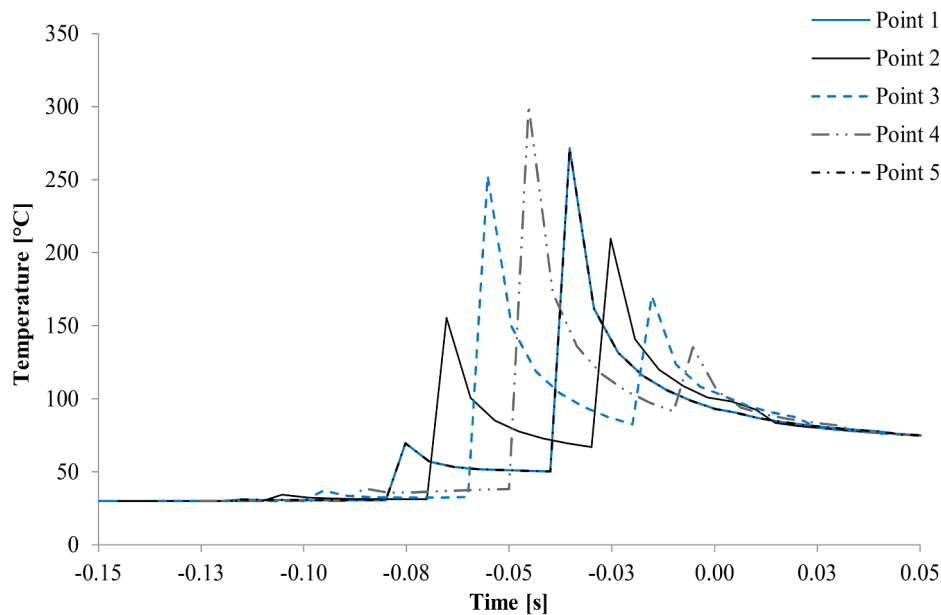
Fig. 13. Temperature history of five surface points, 5 mm apart each, in the case of 25 Hz frequency and 4.75 ms pulse duration at the placement speed of 500 mm/s. (For interpretation of the references to colour in this figure legend, the reader is referred to the web version of this article.)
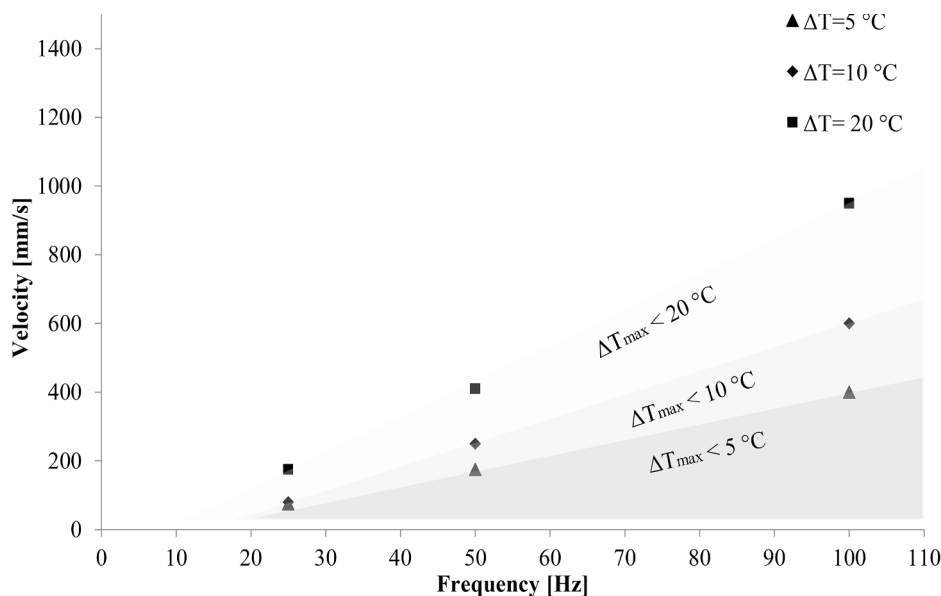

Fig. 14. Frequency-deposition rate process map of flashlamp ATP resulting in differences lower than 5, 10 and 20°C among surface points during the process cycle for 4.4 kW average power.

deploying the model developed to limit the process parameters space appropriately. The fundamental differences with the profiles produced by continuous heating necessitate an understanding of the effect the pulsed operation has on the material transformations occurring during the process. Simulations incorporating material effects can refine further the process map taking into account crystallinity levels, bond strength and thermal degradation effects.

CRediT authorship contribution statement

Anastasios Danezis: Conceptualization, Investigation, Methodology, Software, Formal analysis, Validation, Writing - original draft. **David Williams:** Conceptualization, Writing - review & editing, Supervision. **Michael Edwards:** Investigation, Methodology, Writing - review & editing. **Alexandros A Skordos:** Conceptualization, Writing - review & editing, Funding acquisition, Supervision.

Declaration of Competing Interest

The authors declare that they have no known competing financial interests or personal relationships that could have appeared to influence the work reported in this paper.

Acknowledgements

References

[1] Schledjewski R. Thermoplastic tape placement process-in situ consolidation is reachable. Plast Rubber Comp 2009;38(9–10):379–86.

[2] Lucaszewicz DHJA, Ward C, Potter KD. The engineering aspects of automated prepreg layup: History, present and future. Comp B Eng 2012;43:997–1009.

[3] Khan MA, Mitschang P, Schledjewski R. Parametric study on processing parameters and resulting part quality through thermoplastic tape placement process. J Compos Mater 2013;47(4):485–99.

[4] Pitchumani R, Ranganathan S, Don RC, Gillespie Jr JW, Lamontia MA. Analysis of transport phenomena governing interfacial bonding and void dynamics during thermoplastic tow-placement. Int J Heat Mass Transf 1996;39(9):1883–97.

[5] Sonmez FO, Akbulut M. Process optimisation of tape placement for thermoplastic composites. Compos A: Appl Sci Manuf 2007;38:2013–23.

[6] Tierney JJ, Gillespie Jr J. Crystallization kinetics behavior of PEEK based composites exposed to high heating and cooling rates. Compos Part A: Appl Sci Manuf 2004;35(5):547–58.

[7] Pistor CM, Güçeri SI. Crystallinity of on-line consolidated thermoplastic composites. J Compos Mater 1999;33(4):306–24.

[8] Rosselli F, Santare MH, Güçeri SI. Effects of processing on laser assisted thermoplastic tape consolidation. Compos Part A: Appl Sci Manuf 1997;28(12):1023–33.

[9] Sonmez FO, Hahn HT. Modeling of heat transfer and crystallization in thermoplastic composite tape placement process. J Thermoplast Compos Mater 1997;10(3):198–240.

[10] Tierney J, Gillespie JW. Modeling of heat transfer and void dynamics for the thermoplastic composite tow-placement process. J Compos Mater 2003;37(19):1745–68.

[11] Ranganathan S, Advani SG, Lamontia MA. A non-isothermal process model for consolidation and void reduction during in-situ tow placement of thermoplastic composites. J Compos Mater 1995;29(8):1040–62.

[12] Martin MI, Rodríguez-Lence F, Güemes A, Fernández-López A, Pérez-Maqueda LA. On the determination of thermal degradation effects and detection techniques for thermoplastic composites obtained by automatic lamination. Compos Part A: Appl Sci Manuf 2018;111:23–32.

[13] Grove S. Thermal modelling of tape laying with continuous carbon fibre-reinforced thermoplastic. Composites 1988;19(5):367–75.

[14] Stokes-Griffin CM, Compston P, Matuszyk TI, Cardew-Hall MJ. Thermal modelling of the laser-assisted thermoplastic tape placement process. J Thermoplast Compos Mater 2013;28(10):1445–2146.

[15] Stokes-Griffin CM, Compston P. A combined optical-thermal model for near-infrared laser heating of thermoplastic composites in an automated tape placement process. Compos Part A: Appl Sci Manuf 2015;75:104–15.

[16] Grouve WJB, Warnet LL, Akkerman R. Towards a process simulation tool for the laser assisted tape placement process. In: 14th European conference on composite materials. Budapest; June, 2010.

[17] Orth T, Weimer C, Krahl M, Modler N. A review of the radiative heating in automated layup and its modelling. J Plast Technol 2017;2(2):91–125.

[18] Chern B, Moon TJ, Howell JR. On-line processing of unidirectional fiber composites using radiative heating: I. Model. J Compos Mater 2002;36(16):1905–34.

[19] Hörmann P, Stelzl D, Lichtinger R, Van Nieuwenhove S, Mazón Carro G, Drechsler K. On the numerical prediction of radiative heat transfer for thermoset automated fiber placement. Compos A: Appl Sci Manuf 2014;67:282–8.

[20] Lichtinger R, Hörmann P, Stelzl D, Hinterhölzl R. The effects of heat input on adjacent paths during automated fibre placement. Compos A: Appl Sci Manuf 2015;68:387–97.

[21] Toso YM, Ermanni P, Poulikakos D. Thermal phenomena in fiber-reinforced thermoplastic tape winding process: computational simulations and experimental validations. J Compos Mater 2004;38(2):107–35.

[22] Schledjewski R, Latrille M. Processing of unidirectional fiber reinforced tapes—fundamentals on the way to a process simulation tool (ProSimFRT). Compos Sci Technol 2003;63(14):2111–8.

[23] Chinesta F, Leygue A, Bognet B, et al. First steps towards an advanced simulation of composites manufacturing by automated tape placement. Int J Mater Form 2014;7(1):81–92.

[24] Beyeler EP, Güçeri SI. Thermal analysis of laser-assisted thermoplastic–matrix composite tape consolidation. J Heat Transfer 1988;110(2):424–30.

[25] Agarwal V, Güçeri SI, Mccullough RL, Schultz JM. Thermal characterization of the laser-assisted consolidation process. J Thermoplast Compos Mater 1992;5(2):115–35.

[26] Nejhad NG, Cope RD, Güçeri SI. Thermal analysis of in-situ thermoplastic composite tape laying. J Thermoplast Compos Mater 1991;4(1):20–45.

[27] Maurer D, Mitschang P. Laser-powered tape placement process–simulation and optimization. Adv Manuf Polym Compos Sci 2015;1(3):129–37.

[28] Sarrazin H, Springer GS. Thermochemical and mechanical aspects of composite tape laying. J Comp Mater 1995;29(14):1908–43.

[29] Mantell SC, Springer GS. Manufacturing process models for thermoplastic composites. J Compos Mater 1992;26(16):2348–77.

[30] Kim HJ, Kim SK, Lee WI. A study on heat transfer during thermoplastic composite tape lay-up process. Exp Therm Fluid Sci 1996;13(4):408–18.

[31] Levy A, Heider D, Tierney J Gillespie JW, Lang D. Simulation and optimization of the thermoplastic Automated Tape Placement (ATP) process. In: SAMPE, Baltimore; June 2012.

[32] Stokes-Griffin CM, Compston P. Optical characterisation and modelling for oblique near-infrared laser heating of carbon fibre reinforced thermoplastic composites. Opt Lasers Eng 2015;72:1–11.

[33] Brandt L, Deden D, Fischer FJC, Bruckner F, Dreher P, Williams D, et al. Xenon flashlamp based in-situ automated fibre placement of thermoplastic composites. 22nd international conference on composite materials. 2019.

[34] Brown M, Monnot P, Williams D. Developments in Xenon flashlamp heating for automated fibre placement. Fourth international symposium on automated composites manufacturing. 2019.

[35] Monnot P, Williams D, Francesco M. Power control of a flashlamp-based heating solution for automated dry fibre placement. In: 18th European Conference on Composite Materials. Athens; June, 2018.

[36] Gresho PM, Lee RL. Don't suppress the wiggles-They're telling you something! Comput Fluids 1981;9(2):223–53.

[37] Parker WJ, Jenkins RJ, Butler CP, Abbott GL. Flash Method of determining thermal diffusivity, heat capacity, and thermal conductivity. J Appl Phys 1961;32(9):1679–84.

[38] Lau SK, Almond DP, Patel PM. Transient thermal wave techniques for the evaluation of surface coatings. J Phys D Appl Phys 1991;24:428–36.

[39] Incropera FP, Dewitt DP, Bergman TL, Lavine AS. Fundamentals of Heat and Mass Transfer. 6th ed. John Wiley and Sons; 2007.

[40] Wickern G. Mixed convection from an arbitrarily inclined semi-infinite flat plate – I. The influence of the inclination angle. Intl J Heat and Mass Transf 1989;34(8):1935–45.

[41] Iffländer R. Solid state lasers for materials processing: Fundamental relations and technical realizations. Berlin: Springer; 2001.

[42] Koechner W. Solid state laser engineering. 6th ed. Berlin: Springer; 2006.

[43] Kim SK, Jung BS, Kim HJ, Lee WL. Inverse estimation of thermophysical properties for anisotropic composite. Exp Therm Fluid Sci 2003;27:697–704.

[44] Cogswell FN. Thermoplastic aromatic polymer composites: A study of the structure, processing, and properties of carbon fibre reinforced polyetheretherketone and related materials. Oxford: Butterworth Heinemann; 1992.

[45] TracePro®. www.lambdares.com/tracepro/; 2018.

[46] Hale GM, Query MR. Optical constants of water in the 200-nm to 200-μm wavelength region. Appl Opt 1973;12(3):555–63.

[47] Rakić AD, Djurisic AB, Elazar JM, Majewski ML. Optical properties of metallic films for vertical-cavity optoelectronic devices. Appl Optics 1998;37(22):5722–83.

[48] Satheesh B, Tonejc M, Potakowskyj L, Pletz M, Fauster E, Kaynak B, et al. Peel strength characterisation on ply/ply interface using wedge and T-peel/pull-type tests. Polym Polyme Comp 2018;28(8–9):431–45.

[49] humm3™ – Intelligent heat for Automated Fibre Placement (AFP). www.heraeus.com; 2018.

[50] Thermocouple response times. www.omega.co.uk; 2019.

School of Aerospace, Transport and Manufacturing (SATM)　　　　Staff publications (SATM)

2021-03-13

Heat transfer modelling of flashlamp heating for automated tape placement of thermoplastic composites

Danezis, Anastasios

Elsevier